

Formation mechanism of hierarchical structure of crystal morphology in a sessile droplet

Kouki Morinaga, Marie Tani, and Rei Kurita

Department of Physics, Tokyo Metropolitan University, 1-1 Minami-Osawa, Hachioji-shi, Tokyo 192-0397, Japan



(Received 25 September 2019; published 29 January 2020)

Crystal patterns formed by evaporation play important roles in industrial technologies. Recently, it was found that a concentric pattern and an orchid pattern may be seen when a pinned sessile droplet dries. Due to complex coupling between evaporation and crystallization, the mechanism behind this unique recrystallization phenomenon is yet to be determined. Here, we investigate the formation of these macroscopic patterns using microscopy. Then we show that diffusion-limited aggregation, absorption, and dewetting from the substrate all play a role in its development. In addition, it is found that anisotropy of the core is a key parameter for the pattern formation on a long length scale.

DOI: [10.1103/PhysRevResearch.2.013098](https://doi.org/10.1103/PhysRevResearch.2.013098)

Crystallization on a substrate induced by sessile droplet evaporation is a key physical phenomenon not only for condensed matter physics but also for industrial technologies, including pharmaceutical productions, foods, and architectures [1,2]. When a solution droplet dries, e.g., sodium chloride (NaCl) in water, the solution concentration increases as the solvent evaporates; this is followed by recrystallization of the solute. During this process, it has been found that the size of crystallites is smaller than those formed during precipitation in bulk [3,4]. Smaller crystallites of NaCl have notably different solubility; this may be leveraged, e.g., to suppress salt intake in the human body without changing food taste. We also note that damage to building materials, e.g., bricks near the ocean due to the recrystallization of sea salt, is a major issue [5–7]. A detailed investigation of sessile droplet evaporation is of significant interest in light of a wide range of issues and applications.

The evaporation of droplets with dissolved salt has been investigated [6–14]. It was reported that a concentric pattern may be formed by repeated pinning and slipping during the evaporation of droplets containing L-ascorbic acid [8] and bovine serum albumin [9]. Shahidzadeh *et al.* investigated recrystallization dynamics for different substrates [11]. It was found that crystallites of CaSO₄ are observed at the edge a dried droplet when the substrate is hydrophilic, while a needle-like shape is formed when the substrate is hydrophobic. Such modification of crystal morphologies may have an effect on the macroscopic physical properties, e.g., refractive index, electric conductivity, and mechanical properties [3,4,7,15–20]. Yet, we note that elucidating the specific mechanisms behind such a rich phenomenology is a formidable challenge; recrystallization in a salt solution due to evaporation is a complex phenomenon, with coupling between ma-

terial transport, hydrophobicity, thermal behavior, shrinking, and local concentration [6,8–14].

Recently, we reported the formation of morphology when a drying sessile droplet of sodium bicarbonate solution with colloidal particles is pinned at the edge due to the coffee ring effect [21]. During evaporation of the solvent on a substrate, the colloids are first seen to aggregate at the edge a droplet by a spatially inhomogeneous evaporation rate [22,23]. Then, recrystallization is forced to occur from a thin layer due to the pinning; this leads to the formation of a concentric circle (CC) or an orchid (OR) pattern. OR pattern here refers to the development of large petals radiating growing from the central core at a small number of points. We showed that the CC pattern tends to be formed when the evaporation rate β is high and the initial concentration ϕ_0 is small, while the OR pattern is observed for smaller β and larger ϕ_0 . Although we determined the conditions required for different patterns, the mechanism behind their formation is not yet clear. It is also not obvious whether this pattern formation can be generally observed in other materials. Here, we investigate this recrystallization phenomenon with improved temporospatial resolution and identify a hierarchical structure within the morphology. We also clearly determine that the formation of the hierarchical structure is related to diffusion-limited aggregation (DLA), absorption by the core and dewetting from the substrate. If a solution shows diffusive behaviors with attractive interactions and it has affinity to the crystal, these macroscopic morphologies can be generally formed in a liquid film.

We used sodium bicarbonate (NaHCO₃) with 99% purity purchased from Wako Chemical Industries, Ltd. We put a 20–200 mm³ droplet of the solution on a cover glass; recrystallization occurs on evaporation. Initial weight fraction is in the range from $\phi_0 = 5.0 \times 10^{-4}$ to 0.050. The saturation concentration of NaHCO₃ in water is 0.087. To investigate macroscopic pattern formation with a combined coffee ring effect, polystyrene latex particles (Magsphere Co.) with 0.052 μm diameter were mixed into the solution at a volume fraction of 0.01%. The sample temperature T was controlled with a transparent hot stage (Blast Co.). The humidity

was measured for every experiment. We observed the time evolution of the pattern formation using an optical microscope (Nikon ECSROPSE-TS100), a fluorescence microscope (Nikon ECLIPSE Ni-E), and a polarized microscope (Nikon ECLIPSE LV100ND). For the fluorescence microscopy, we used rhodamine 6G for dye. The droplet size over time was tracked with a digital camera (Panasonic, HC-W570M). The mass of the solution was measured using a digital balance with an accuracy of ± 0.01 mg (AS ONE, IUW-200D). The evaporation rate β was about 3.0×10^{-3} mg/s to 9.0×10^{-3} mg/s.

During evaporation, the pinned droplet becomes thinner and is transformed into a thin liquid film. Note that the droplet shrinks and keeps the cap shape if it is not pinned. As the water evaporates, the concentration of the solution increases. Importantly, the concentration at the edge becomes higher than in the center since the macroscopic flow is larger than diffusive flow. We estimate the Peclet number $Pe = RU/D$ for inhomogeneities in the concentration, where R , U , and D are the radius, typical velocity, and diffusion constant, respectively. The Peclet number represents the ratio of advection to diffusion. U can be estimated as $\beta/A(t)$ where $A(t)$ is the square of the cylinder of the droplet [11,21]. We use the D of water (1.0×10^{-9} m²/s), which is of similar order to the diffusion constant of each ion. We obtain $Pe = 4.8$ for $\beta = 3.0 \times 10^{-3}$ mg/s. Thus, recrystallization starts at the edge and only occurs in the center at a later time [21]. Then we define a crystallization time t_X when the solution at the edge crystallizes; we also define ϕ_X and h_X as the mean concentration and height at t_X , respectively. We estimated the mass fraction at the beginning of the crystallization ϕ_X as

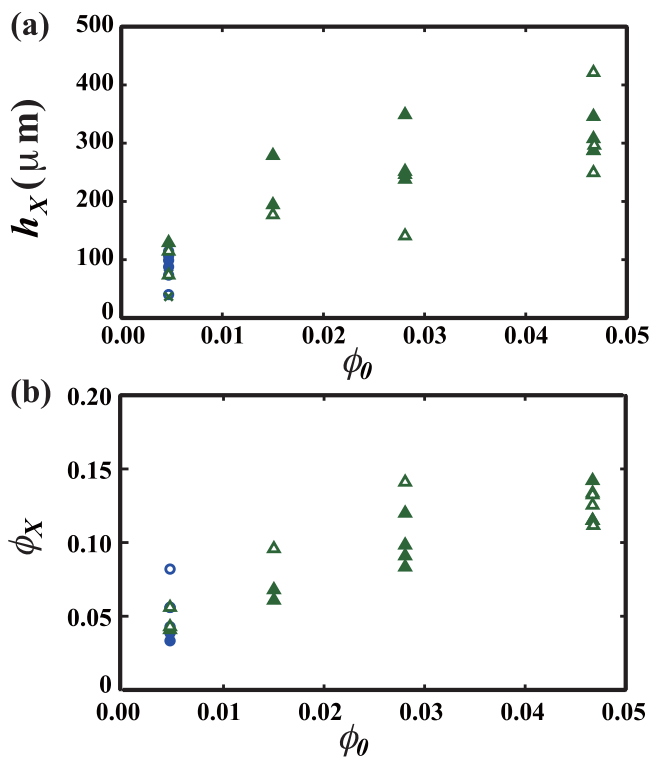


FIG. 1. (a) h_X and (b) ϕ_X as functions of ϕ_0 . Open triangles and open circles correspond to results in the OR pattern and CC pattern at 20 °C. Filled symbols correspond to those at 30 °C.

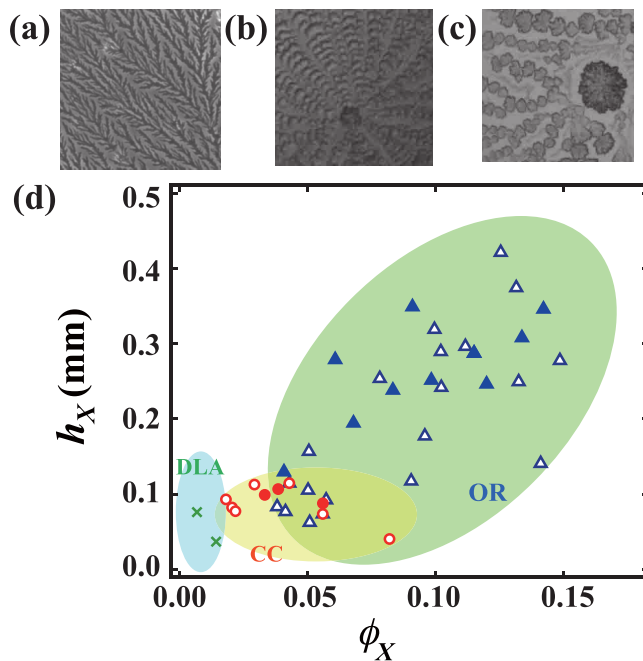


FIG. 2. Microscopy image of the (a) dendritic pattern, (b) CC pattern, and (c) OR pattern. Image sizes are $500 \mu\text{m} \times 500 \mu\text{m}$. (d) Patterns as functions of h_X and ϕ_X . Crosses and open symbols correspond to the results at $T = 20^\circ\text{C}$. Filled symbols correspond to the results at $T = 30^\circ\text{C}$.

m_s/m_X , where m_s and m_X are the mass of the solute and the mass of the solution at the beginning of the crystallization. m_X was measured by a digital balance whose accuracy is ± 0.01 mg (AS ONE, IUW-200D). We also estimated the height of the sample at the beginning of the crystallization h_X by using the weight and the radius of the sessile droplet. When the crystallization started, h_X is quite small. Thus we can approximate the shape of the droplet as the cylinder. Thus h_X can be estimated by $m_X/(\rho\pi r^2)$, where ρ and r are the density and the radius of the sessile droplet. Here it is found that ϕ_X and h_X correlate positively with ϕ_0 as shown in Fig. 1; we note that the reason for the relation between ϕ_X and ϕ_0 is unclear [11].

Next, we focus on the morphology at the center of the droplet, noting that a cluster of aggregates can be observed near the edge. We observe three distinct morphologies, a dendritic pattern, a concentric circle (CC) pattern, and an orchid (OR) pattern, as shown in Figs. 2(a)–2(c). We find that the CC and the OR patterns have a large core consisting of an aggregated dendritic pattern. Figure 2(d) shows which crystal morphology is seen for different ϕ_X and h_X . Open and filled symbols correspond to the patterns at 20 °C and 30 °C, respectively. For small ϕ_X , we observe a dendritic pattern [Fig. 2(a)]; we estimate a fractal dimension D using the box-counting method [24] of $D = 1.83 \pm 0.10$ (Fig. 3). The error in D is estimated by measuring 10 independent samples. This is similar to the fractal dimension ($D = 1.71$) seen for diffusion-limited aggregation (DLA) [25,26]. Thus, the crystal grows following DLA for smaller ϕ_X , consistent with the general observation of DLA in dilute systems. Meanwhile, the CC pattern is observed for smaller h_X ; the OR pattern

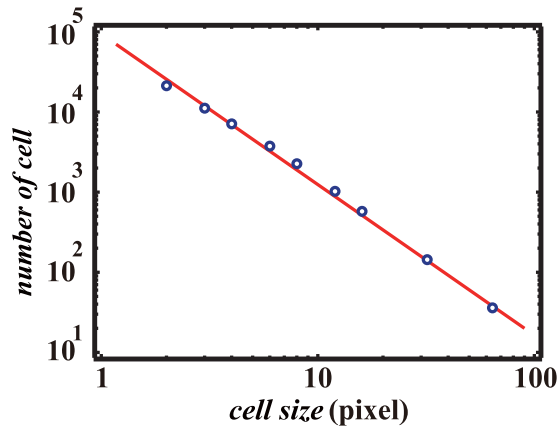


FIG. 3. Computing the fractal dimension with the box-counting method. We obtained $D = 1.83 \pm 0.10$.

is formed for larger h_X and ϕ_X . We note that the boundary between CC and OR is marginal; this is discussed later.

Next, we consider the formation dynamics of the CC and OR patterns. We find that a core is formed first, and CC or OR patterns are formed around it. Figures 4(a1)–4(a3) show microscopy images of the time evolution of the CC pattern formation. Subsequent rings are formed sequentially in the same manner as the first ring. We confirm that the dynamics of the CC pattern formation is always reproduced in 10 independent samples. This formation dynamics is distinct from the stick and slip dynamics [23]. Figures 4(b1)–4(b3) show microscopy images of the time evolution of the OR pattern. d is defined as the distance from the emergence point to the end point. Figure 5 shows the time evolution of d . Open circles represent one petal growing and filled circles represent the next petal growing. The petal grows with time at the early stage; however the growing is arrested at some time. After arrest, the next petal grows from a neighboring location. We always observe those dynamics in the OR pattern formation when we observe 10 petals growing in 10 distinct samples.

Here we investigate the microscopic internal structure of the core. Figure 6(a) shows an image obtained by the polarized microscope with a sensitive tint plate. The purple color corresponds to no birefringence; on the other hand, red and blue colors correspond to birefringence of the crystal. We find that the core shows a Maltese cross, which is a typical pattern for spherulite. The spherulite is usually formed by the dendritic pattern (for example, polymer crystals). Meanwhile, a single crystal is a single color as shown in Fig. 6(b). Thus, it is likely that the internal structure is dendritic rather than the single crystal. The Maltese cross of the core is always observed regardless of whether it is in the OR pattern or in the CC pattern. Thus, we consider the entire structure as possessing a hierarchy; i.e., the core is a higher-order structure consisting of the dendritic pattern.

We also track pattern evolution by the fluorescence microscope. We mix a small amount of rhodamine into the solution. Figures 7(a)–7(c) show the time evolution of growth of a core at (a) 123.2 s, (b) 124.7 s, and (c) 128.3 s after t_X . The brightness represents the amount of the rhodamine. The core has higher brightness than the solution. The crystal excludes

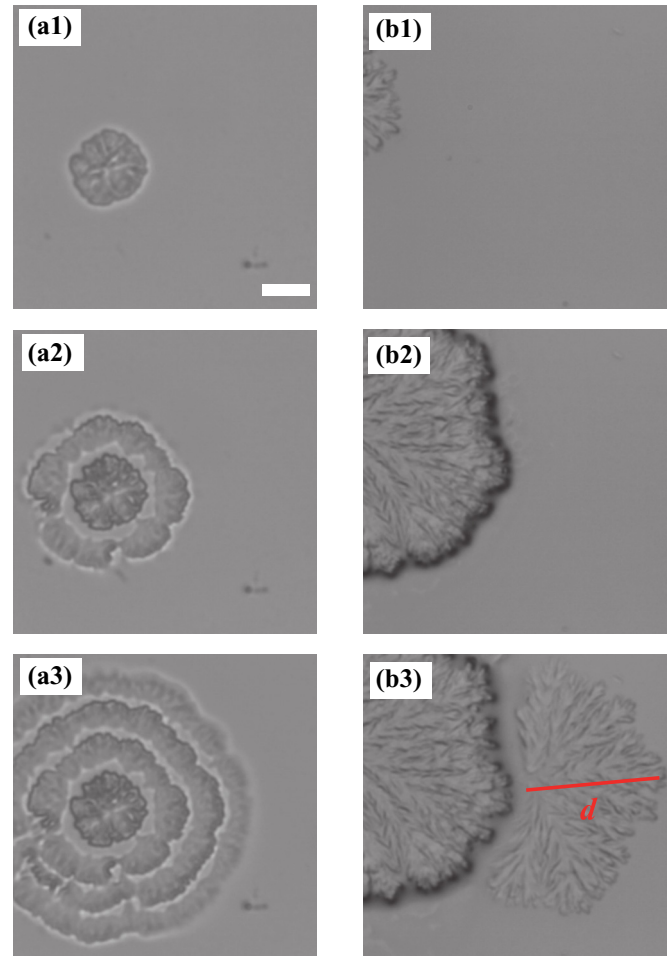


FIG. 4. Time evolution of (a1)–(a3) CC and (b1)–(b3) OR patterns. The CC pattern is formed at $\phi_0 = 0.046$ at 30°C and $R_h = 62\%$. The OR pattern is formed at $\phi_0 = 0.046$ at 23°C and $R_h = 56\%$. The white bar is $20\ \mu\text{m}$. Times are (a1) 0 s, (a2) 0.33 s, and (a3) 0.67 s; and (b1) 0 s, (b2) 7.3 s, and (b3) 14.5 s.

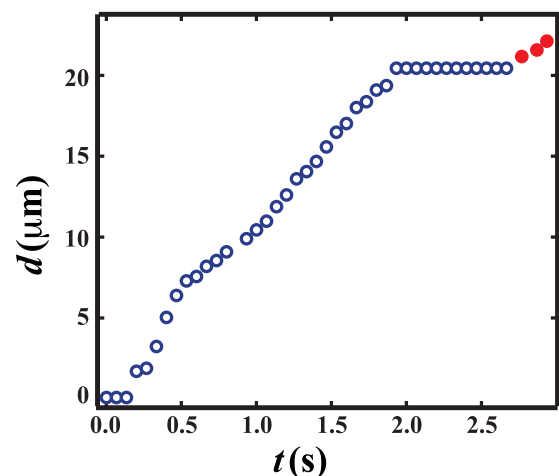


FIG. 5. Time evolution of d . Open circles represent one petal growing and filled circles represent the next petal growing. The petal grows with time at the early stage; however the growing is arrested at some time. After that, the new petal grows from the petal.

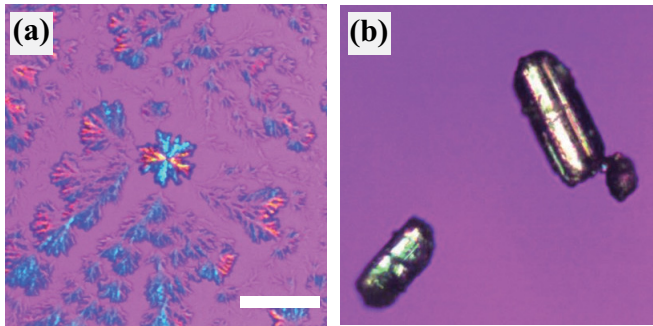


FIG. 6. (a) A core of the OR pattern and (b) a single crystal obtained by the polarized microscope with a sensitive tint plate. The white bar represents $100\ \mu\text{m}$. Purple color corresponds to no birefringence; on the other hand, red and blue colors correspond to birefringence of the crystal. The core shows a Maltese cross, while the single crystal has a single color. It is likely that the internal structure of the core is dendritic rather than a single crystal.

rhodamine and the concentration becomes higher [Fig. 7(a)]. Here, it is found from the images that there is space inside the core. This also supports that the core might be a dendritic pattern rather than the single crystal. Then we find that the core near the interface becomes brighter [Fig. 7(b)]. After that, the center of the core becomes brighter [Fig. 7(c)]. Figure 7(d) shows the time evolution of the intensity along the solid arrow

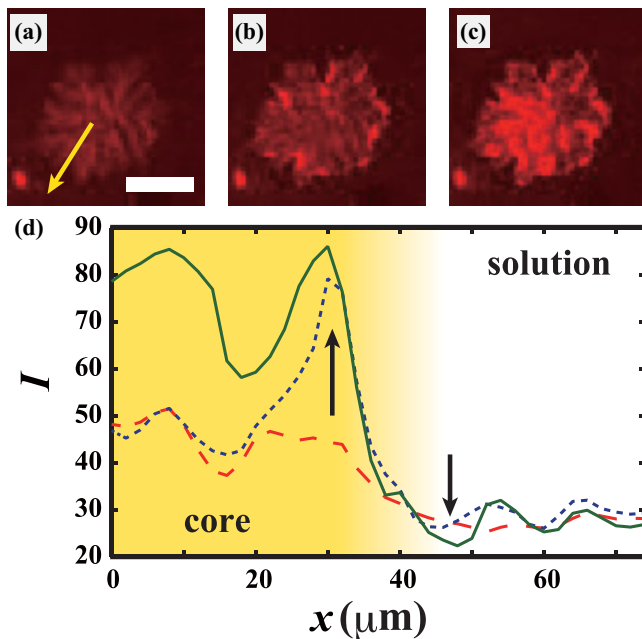


FIG. 7. Time evolution of the growth of the core at (a) 123.2 s, (b) 124.7 s, and (c) 128.3 s after t_X obtained by the fluorescence microscope. The white bar represents $20\ \mu\text{m}$. We find that the core becomes brighter from the inner edge (b) to the center (c). (d) Time evolution of the intensity I along a solid arrow in (a). Red, blue, and green lines represent I at 123.2 s, 124.7 s, and 128.3 s after t_X , respectively. I increases near the interface at first and then I increases inside the core. Meanwhile, I decreases outside the core. This suggests that the solution with rhodamine is absorbed by the core.

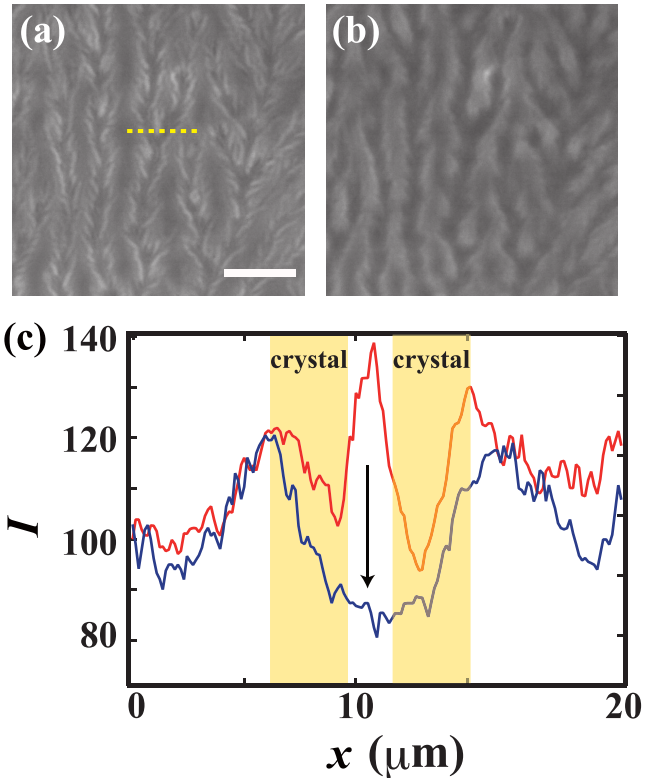


FIG. 8. The wetting dynamics in the dendritic pattern. We set the time we inject the solution as $t = 0$ s. (a) $t = 0$ s and (b) $t = 6.6$ s after we injected the solution. (c) Time evolution of the image intensity at the dashed line in (a). Red and blue lines represent the intensity at $t = 0$ and $t = 6.6$ s, respectively. The crystal region and the region between the branches wet quickly. The white bar corresponds to $20\ \mu\text{m}$.

in Fig. 7(a). Red, blue, and green lines represent I at 123.2 s, 124.7 s, and 128.3 s after t_X , respectively. We confirm that I increases from the interface to the center of the core, while I decreases outside the core. This suggests that the solution is absorbed by the core. These behaviors are always reproduced regardless of the OR pattern or the CC pattern.

To confirm that this is indeed occurring, we observe the wetting dynamics of the solution to the dendritic pattern [Fig. 8(a)]. We put a small droplet of saturated solution at the edge of the dried dendritic pattern. First, the solution rapidly spreads over the crystal, and we see the solution filling in the gaps between the branches in the dendritic pattern [see Fig. 8(b)]. The red and blue lines in Fig. 8(c) show the image intensity along the dashed line in Fig. 8(a) at $t = 0$ s and 6.6 s. It is clear that the solution begins to bridge the region between the branches of the dendritic pattern. From this, we see that the wettability of the solution on the crystal is high, and that there is a capillary force at work between the branches. When ϕ_X is large, the density of the dendritic branch becomes higher [27]. Thus, this suggests that the dense dendritic pattern at the core might be formed by the absorption of the solution by the pattern at larger ϕ_X .

We also consider the wetting of the solution to a dried OR pattern by again putting a small droplet of saturated solution including rhodamine on the pattern. Figures 9(a)–9(c)

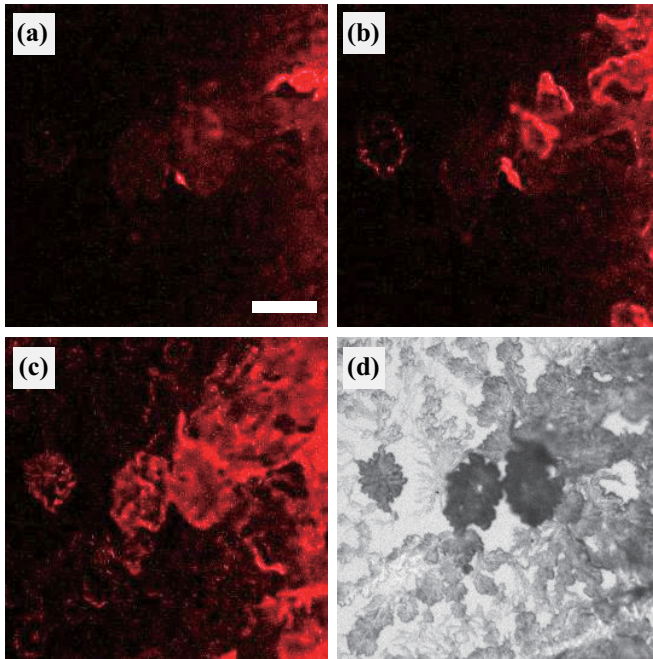


FIG. 9. Wetting dynamics in the dried OR pattern at (a) 212.9 s, (b) 243.3 s, and (c) 293.2 s after injection observed by the fluorescence microscope. We put a small droplet of saturated solution with rhodamine at the right of the image. (d) The image after the wetting experiment obtained by the phase contrast microscope. The positions of (a)–(d) are same and the white bar in (a) represents $20\ \mu\text{m}$. The solution rapidly spreads from the right to the left of the image via the petals. This suggests that the petals connect to neighboring petals.

show the time evolution of the wetting dynamics at (a) 212.9 s, (b) 243.3 s, and (c) 293.2 s after injection observed by the fluorescence microscope, and Fig. 9(d) is an image obtained by the phase contrast microscope after the wetting experiment. When the solution comes into contact with the dried OR pattern [Fig. 9(a)], the solution quickly spreads into the petals [Figs. 9(b) and 9(c)]. Meanwhile the intensity around the petals remains quite low. This suggests that there is no invisible crystallite around the petals and that the solution detaches from the substrate due to absorption into the crystal region. In addition, we find that petals connect to neighboring petals, and that the solution spreads via these junctions.

In contrast, for the dried CC pattern, we find that the solution spreads slowly over the pattern (see Fig. 10). The solution spreads isotropically [see Figs. 10(a)–10(c)], regardless of the existence of the pattern inside the droplet. This means that the solution propagates to the substrate region similarly to the crystal region. We note that this dynamics is different from the case in the OR pattern. We also note that the wetting dynamics is significantly slower than in the OR pattern. Hence, the crystalline rings are separated from each other due to dewetting of the solution from the substrate.

Next, we consider a key parameter for distinguishing CC and OR patterns. In the OR pattern, the petals are partially connected, while the rings in the CC are separated at approximately the same distance from the center, all the way around. Thus, we look for a relationship between the isotropy of the core (or radial symmetry) and the pattern. To estimate

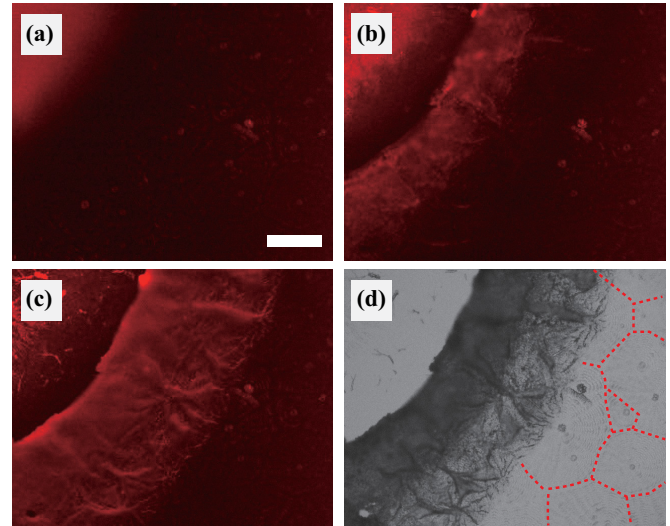


FIG. 10. Wetting dynamics in the dried CC pattern at (a) 12.2 s, (b) 129.8 s, and (c) 264.9 s after injection observed by a fluorescence microscope. We add a small droplet of saturated solution with the rhodamine at the left of the image. (d) The image after the wetting experiment obtained by a phase contrast microscope. The positions in (a)–(d) are the same and the white bar in (a) represents $20\ \mu\text{m}$. Dotted lines in (d) show the boundary of each CC pattern.

the isotropy of the core, we compute $\langle r \rangle$ and Δr , where r is the distance between the center of mass of the pattern and the interface. $\langle r \rangle$ and Δr are the mean of r and the standard deviation of r , respectively. Figure 11 shows the morphology diagram as a function of Δr and $\langle r \rangle$. Open circles and open triangles correspond to the CC and OR patterns obtained when $\beta \sim 3.0 \times 10^{-3}\ \text{mg/s}$, respectively. We also compute Δr and $\langle r \rangle$ for those obtained when $\beta \sim 10^{-1}\ \text{mg/s}$ (filled symbols). Interestingly, the pattern formation seems independent of the core size. It is only correlated with core isotropy. If absorption to the core occurs isotropically, then dewetting should also be isotropic, particularly when the core is close to a circular shape. On the other hand, an anisotropic core features more

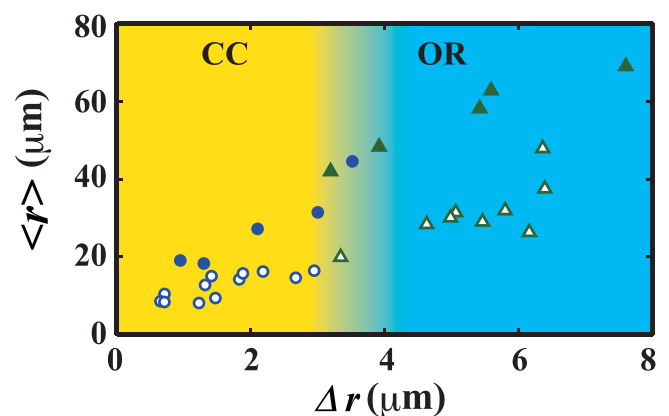


FIG. 11. Pattern diagram for $\phi_x > 0.03$ as functions of $\langle r \rangle$ and Δr . Open circles and open triangles correspond to CC and OR patterns obtained when $\beta \sim 3.0 \times 10^{-3}\ \text{mg/s}$, respectively. Filled circles and filled triangles correspond to CC and OR patterns obtained for $\beta \sim 10^{-1}\ \text{mg/s}$, respectively. This suggests that Δr is the key parameter separating CC and OR patterns, not $\langle r \rangle$.

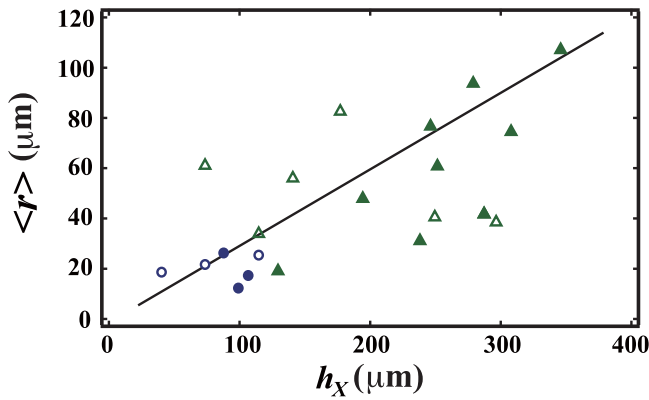


FIG. 12. $\langle r \rangle$ as a function of h_X . Open circles and open triangles correspond to CC and OR patterns obtained when $\beta \sim 3.0 \times 10^{-3}$ mg/s, respectively. Filled circles and filled triangles correspond to CC and OR patterns obtained for $\beta \sim 10^{-1}$ mg/s, respectively. $\langle r \rangle$ has a positive relation with h_X . The solid line is a guide for the eye. It is natural since the timing for detachment of the solution from the substrate becomes later when h_X is larger, resulting in a larger $\langle r \rangle$.

irregularities; a tip, where the dendritic is sparser, will result in less absorption compared with a bottom, leaving the solution to remain locally without detaching from the substrate. In fact, we observe that the bottom becomes brighter than the tip, as shown in Fig. 7(b). The next petal grows from the tip point as a result. This is why a CC pattern is formed when the core is isotropic, while an OR pattern is formed when the core is anisotropic.

The relationship between Fig. 2(d) and the parameter $\langle r \rangle$ deserves discussion. When h_X is large, the timing for detachment of the solution from the substrate becomes later, resulting in a larger $\langle r \rangle$ (see Fig. 12). It is also reasonable that Δr becomes larger with the growth of core size; in fact, Δr has positive relation with $\langle r \rangle$ for similar β (see Fig. 11). This is consistent with the observation of an OR pattern for larger h_X (see Fig. 2). Meanwhile, when β is quite large, the core becomes large although Δr remains small. This is why we see a CC pattern instead for large β [21]. The reason for this is not yet clear, however.

Finally, we show a schematic of the hierarchical structures formed from a sessile droplet in Fig. 13. The smallest of these is the monoclinic crystal system of sodium bicarbonate. This goes on to form a dendritic structure via diffusion-limited aggregation (DLA) since the solution is relatively dilute. The amount of solution decreases in the dendritic structure as the solute transforms into a dense crystal. Gradually, the solution is absorbed into the dendritic structure by capillarity. We

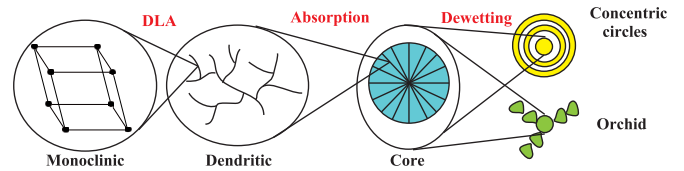


FIG. 13. Schematic of the hierarchical structures formed from a sessile droplet. In a sodium bicarbonate solution, the smallest of these is the monoclinic crystal structure. A dendritic structure is formed via a DLA process since the solution is dilute during recrystallization. A core is formed due to wetting of the solution to the crystal. Subsequently, larger patterns like the CC and OR patterns are created by dewetting of the solution from the substrate. A CC pattern is formed when the core is isotropic, while an OR pattern is observed if the core is anisotropic.

speculate that the dense dendritic structure of the core is formed due to this absorption. When the core is isotropic, the solution is isotropically detached from the substrate. This leads to the formation of the next crystalline ring, eventually resulting in a CC pattern. On the other hand, if the core is anisotropic the solution wets to the core in localized regions; the next petal grows from these locations, forming an OR pattern. We note that DLA, capillarity, and dewetting require diffusion, attractive interactions, affinity to the crystal, and a large wetting angle to the substrate. They are ubiquitously observed in many systems; thus, it is clear that this hierarchical structure may be observed generally.

To summarize, we investigated the mechanisms behind macroscopic pattern formation in drying pinned sessile droplets. We directly observed the absorption of the solution at the growth front of the pattern. We also investigated the wetting dynamics of the solution to the dried macroscopic pattern, confirming that the crystal has good affinity to the solution. In addition, we find that the petals in the OR pattern are connected, while the rings in the CC pattern are separated due to dewetting of the solution from the substrate. The hierarchical structure is thus a result of DLA, capillary forces, and dewetting from the substrate. We also find that the CC pattern is formed when the core is isotropic, while an OR pattern is formed when the core is anisotropic. Although the crystallization dynamics on the small scale is nearly identical for all cases, the morphology on the long length scale is distinct due to anisotropy of the core.

R.K. was supported by JSPS KAKENHI (Grant No. 17H02945).

[1] K. Kelton and A. L. Greer, *Nucleation in Condensed Matter: Applications in Materials and Biology* (Elsevier, Oxford, UK, 2010).
 [2] P. G. Debenedetti, *Metastable Liquids* (Princeton University Press, Princeton, 1997).
 [3] X. Wu, G. Wang, L. Zhao, D. Zeng, and Z. Liu, *Comput. Mater. Sci.* **117**, 286 (2016).

[4] M. Quilaqueo and J. M. Aguilera, *Food Res. Int.* **84**, 143 (2016).
 [5] S. Taber, *Am. J. Sci.* **41**, 532 (1916).
 [6] C. Rodriguez-Navarro and E. Doehne, *Earth Surf. Processes Landforms* **24**, 191 (1999).
 [7] S. Gupta, L. Pel, M. Steiger, and K. Kopinga, *J. Cryst. Growth* **410**, 7 (2015).

- [8] M. Ito, M. Izui, Y. Yamazaki, and M. Matsushita, *J. Phys. Soc. Jpn.* **72**, 1384 (2003).
- [9] T. A. Yakhno, *Phys. Chem.* **1**, 10 (2011).
- [10] K. Sefiane, *Adv. Colloid Interface Sci.* **206**, 372 (2014).
- [11] N. Shahidzadeh, M. F. Schut, J. Desarnaud, M. Prat, and D. Bonn, *Sci. Rep.* **5**, 10335 (2015).
- [12] N. Shahidzadeh-Bonn, S. Rafai, D. Bonn, and G. Wegdam, *Langmuir* **24**, 8599 (2008).
- [13] P. Vázquez, C. Thomachot-Schneider, K. Mouhoubi, G. Fronteau, M. Gommeaux, D. Benavente, V. Barbin, and J.-L. Bodnar, *Infrared Phys. Technol.* **71**, 198 (2015).
- [14] V. Soulie, S. Karpitschka, F. Lequien, P. Prene, T. Zemb, H. Moehwald, and H. Riegler, *Phys. Chem. Chem. Phys.* **17**, 22296 (2015).
- [15] K. G. Libbrecht, *Reg. Prog. Phys.* **68**, 855 (2005).
- [16] H. Honjo, S. Ohta, and M. Matsushita, *Phys. Rev. A* **36**, 4555 (1987).
- [17] R. Kobayashi, *Phys. D (Amsterdam)* **63**, 410 (1993).
- [18] M. Moncada, C. Astete, C. Sabliov, D. Olson, C. Boeneke, and K. J. Aryana, *J. Dairy Sci.* **98**, 5946 (2015).
- [19] N. Oikawa and R. Kurita, *Sci. Rep.* **6**, 28960 (2016).
- [20] R. Kurita, *Sci. Rep.* **7**, 6912 (2017).
- [21] K. Morinaga, N. Oikawa, and R. Kurita, *Sci. Rep.* **8**, 12503 (2018).
- [22] A. G. Marin, H. Gelderblom, D. Lohse, and J. H. Snoeijer, *Phys. Rev. Lett.* **107**, 085502 (2011).
- [23] Y.-J. Chen, K. Suzuki, H. Mahara, K. Yoshikawa, and T. Yamaguchi, *Appl. Phys. Lett.* **102**, 041911 (2013).
- [24] B. Klinkenberg, *Math. Geol.* **26**, 23 (1994).
- [25] D. A. Weitz and M. Oliveria, *Phys. Rev. Lett.* **52**, 1433 (1984).
- [26] F. Barra, B. Davidovitch, A. Levermann, and I. Procaccia, *Phys. Rev. Lett.* **87**, 134501 (2001).
- [27] M. Uwaha and Y. Saito, *J. Phys. Soc. Jpn.* **57**, 3285 (1988).